Supporting Information

Self-patterning of Liquid Field's Metal for Enhanced Performance of Two-dimensional Semiconductors

Kwanghee Han[1,2†], Heeyeon Lee[1†], Minseong Kwon[1,3], Vinod Menon[2], Chaun Jang[3],

and Young Duck Kim[1,4*]

[1]Department of Physics, Kyung Hee University, Seoul, 02447, Republic of Korea.

[2]Department of Physics, City College of New York, New York, NY, 10031, USA.

[3] Center for Spintronics, Korea Institute of Science and Technology, Seoul, 02792, Republic of Korea

[4]Department of Information Display, Kyung Hee University, Seoul, 02447, Republic of Korea.

[†]Equally contributed

*Corresponding author E-mail: ydk@khu.ac.kr

Supporting Note 1. Additional device test with a thinner flake device.

To investigate the potential of this phenomenon, we made other samples with thinner flakes. In Fig. S1a, there is an optical image of one of the devices. We measure the AFM to define its thickness. According to the AFM data in Fig. S1b and S1c, the device has ~ 8 nm thickness corresponding to around 10 layers of WSe_2. The mobility of TMDC-based devices is known to depend on layer thickness. Devices with fewer layers typically exhibit lower mobility due to inadequate screening of substrate-induced scattering effects[1]. On the other hand, devices with thicker layers (more than 15 layers) tend to show increased resistance, primarily due to c-axis access resistance[2]. Thus, our new device is in the proper range of thickness to prevent both the substrate impact and c-axis resistance.

We measured this sample using the same method and compared the results to investigate the Field's metal propagation effect. Figures S2a and S2b show optical images before and after the formation of the Field's metal electrodes. The transfer characteristics (Fig. S2c, S2d) demonstrate a significant reduction in resistance following the self-propagation process. Additionally, the output characteristics show that the current flows more efficiently after the formation of the Field's metal electrodes (Fig. S2e, S2f).

Additionally, we performed mobility calculations for an additional device with ~ 40 nm WSe_2 flakes. Figure S3 illustrates the transfer characteristics and the calculated field-effect mobility of the device. Figures S3a and S3b show that the current increases significantly after the self-propagation process in both the 2 μm and 3 μm channel lengths. For the 3 μm channel, at a gate voltage of 60 V, the current rises from 0.25 nA to 30.5 μA, which represents an enhancement by a factor of 92,424. Moreover, this process leads to a substantial improvement in the on/off current ratio (I_{ON}/I_{OFF}), increasing from approximately 25 to around 71,608.

As shown in S3c and S3d, the mobility also increases from $\sim 0.1\, cm^2/V \cdot s$ to $20 \sim 30\, cm^2/V \cdot s$. It exceeds recently reported mobilities for Chromium and Gold metal contacts with WSe$_2$, which fall $1.838\, cm^2/V \cdot s$[3]. Although the mobility from the contact between WSe$_2$ and Cr/Au electrodes is relatively low, our results confirm that our approach significantly enhances electrical properties.

Based on the results from devices thinner than 10 nm, we conclude that our approach effectively reduces contact resistance by improving the intrinsic interfacial contact. Therefore, introducing the self-propagation effect in high-quality devices will be a breakthrough in overcoming contact resistance challenges in 2-dimensional semiconductor devices.

Supporting Note 2. Uniformity of Field's metal electrodes

To investigate the uniformity of the Field's metal electrodes, we perform SEM imaging to compare the width of electrodes before and after self-propagating. Figure S4a and S4b show the SEM images before and after forming the Field's metal electrodes. To quantify the lateral expansion, we obtain line profiles of electrodes width from SEM images. Figure S4c represents the lateral expansion which is generally less than $\sim$ 40 nm. For more precise comparison, we plot it with error bars to see the range of the width after self-propagation. For example, 240 nm width was increased to 250 nm which is 4.17 %.

Additionally, we performed close SEM images and AFM data. Figure S5a and S5b show the surface of Field's metal electrodes. In Figure S5c, the surface roughness information can be obtained by AFM measurement. The box with white dashed lines represents the Field's metal electrodes on the WSe$_2$ surface. The average thickness in the box is 347.8 nm and RMS roughness (R_q) is 85.23 nm. Figure S5d represents the AFM line profile from red line in Fig. R3c. Thickness of electrode was increased to $\sim$ 400 nm after self-propagation.

Supporting Note 3. Self-propagation driving source test

It is important to figure out the exact driving source for spreading. Based on our additional controlled experiments, the Field's metal is spread on metal surfaces. So, the original electrodes make alloys with the melted liquid metal while heat annealing. We confirmed that it does not happen on the slide glass or SiO2 substrates with additional test.

This process is different from other methods in previous research such as rolling and applying voltage. First, it is not from the external force. We didn't use any roller or apply strain on the samples. Secondly, it is not from the external voltage. Previous research show that applying voltage can control the directional flow of liquid metals[4,5]. However, we didn't use any external voltage source to induce propagation. Lastly, the pressure difference between inside and outside of the Field's metal is not the reason. If that is the reason, the Field's metal would spread through the entire substrate not just on the electrodes. In addition, we confirm the self-propagation happens even at the ambient pressure condition (Figure S6). It proves that pressure is not the source of self-propagation.

Therefore, we consider this phenomenon as a new physical property of liquid metals which can form new alloys with metal surfaces by heating. We strongly believe our work will be the starting point of investigating an interesting phenomenon.

Supporting Note 4. Highest resolution of Field's metal electrodes

To figure out the maximum resolution, we conducted an additional experiment to determine the maximum achievable resolution. For this, we fabricated electrodes with 200 nm widths using E-beam lithography and E-beam evaporation. In Figure S7, 200 nm scale Field's metal electrodes

are successfully constructed by self-propagation. Since this method relies on the original electrode design, we believe it has even greater potential for achieving higher resolution if smaller passive electrodes can be fabricated. Therefore, compared to other methods for creating liquid metal electrodes[6–9], this approach represents a significant breakthrough in achieving high-resolution electrodes.

Supporting Note 5. The field effect mobility calculation

To analyze the electrical performance after self-propagation, we compare the field effect mobility in Figure 4d of manuscript. For the detailed calculation, we used the equation for the field effect mobility, $\mu_{FE} = \left[\dfrac{dI_d}{dV_G}\right] \times \left[\dfrac{L}{WC_iV_{DS}}\right]$, where W is the channel width, L is the channel length, and C_i is the capacitance between channel and back gate per unit area.

For example, there are transfer characteristics in Figure S8. The first thing we do is to extract $\dfrac{dI_d}{dV_G}$ from the slope in the graph. In Fig. S8b, we can get information of $\dfrac{dI_d}{dV_G} = 0.127\ \mu A/V$ with channel length 4 μm from dashed lines. Based on all the parameters ($C_i = \varepsilon_0 \times \dfrac{\varepsilon_r}{d} = 1.21 \times 10^{-8}F/cm^2$; $\varepsilon_0 = 8.85 \times 10^{-12}F/m$, $\varepsilon_r = 3.9$, $d = 285\ nm$), the field effect mobility is $\mu_{FE} = \left[\dfrac{dI_d}{dV_G}\right] \times \left[\dfrac{L}{WC_iV_{DS}}\right] = 5.97cm^2/V \cdot s$.
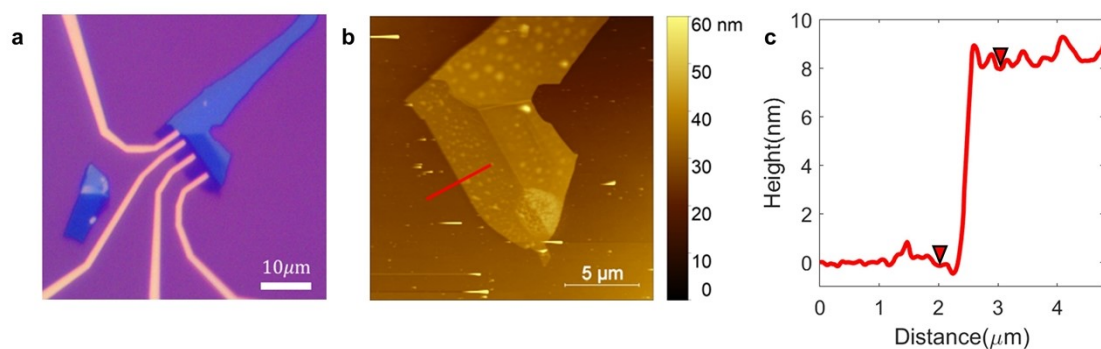
Figure S1 | Sample information for a thinner flake device. (a) Optical image of additional WSe$_2$ device with ~ 8 nm thickness flake. **(b)** AFM image and **(c)** AFM line profile of the red line.
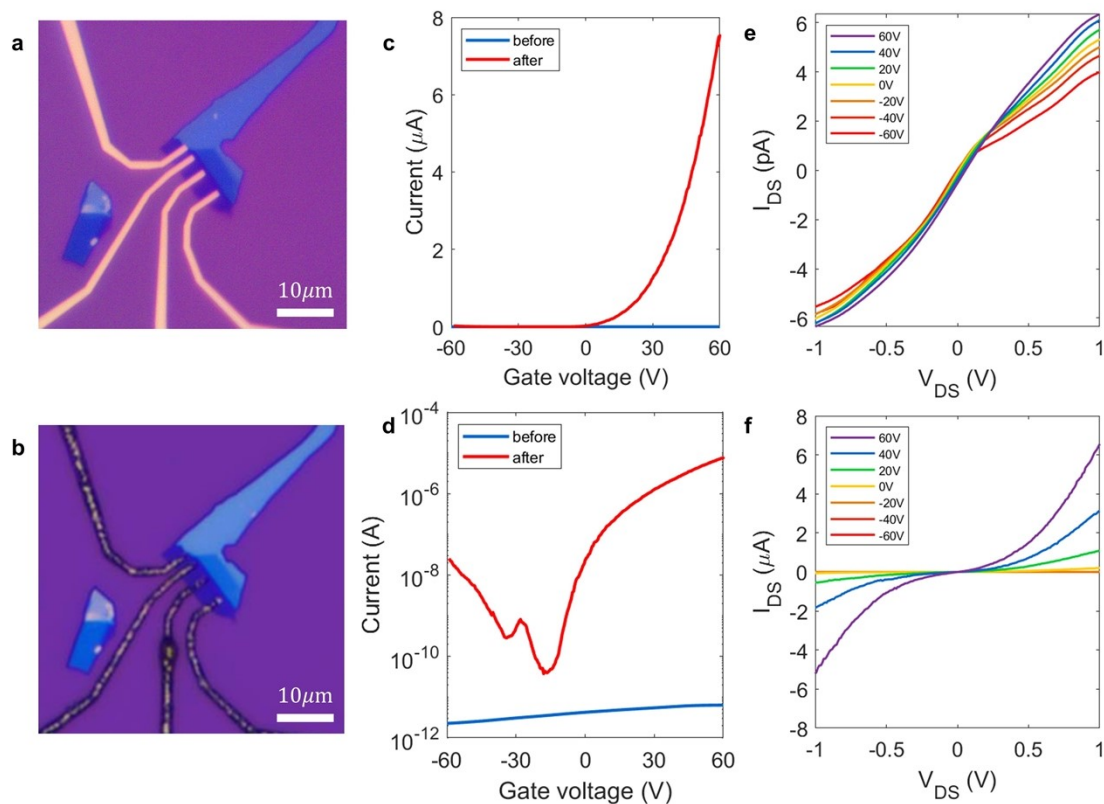
Figure S2 | Electrical characteristic comparison for the thinner device. a-b, Optical image of ~ 8 nm thickness device before and after the process. **(c)** of before and after self-propagation of Field's metal and **(d)** its log scale plot. **e-f,** Output characteristics ($I_{DS} - V_{DS}$) before and after

forming field's metal electrodes.
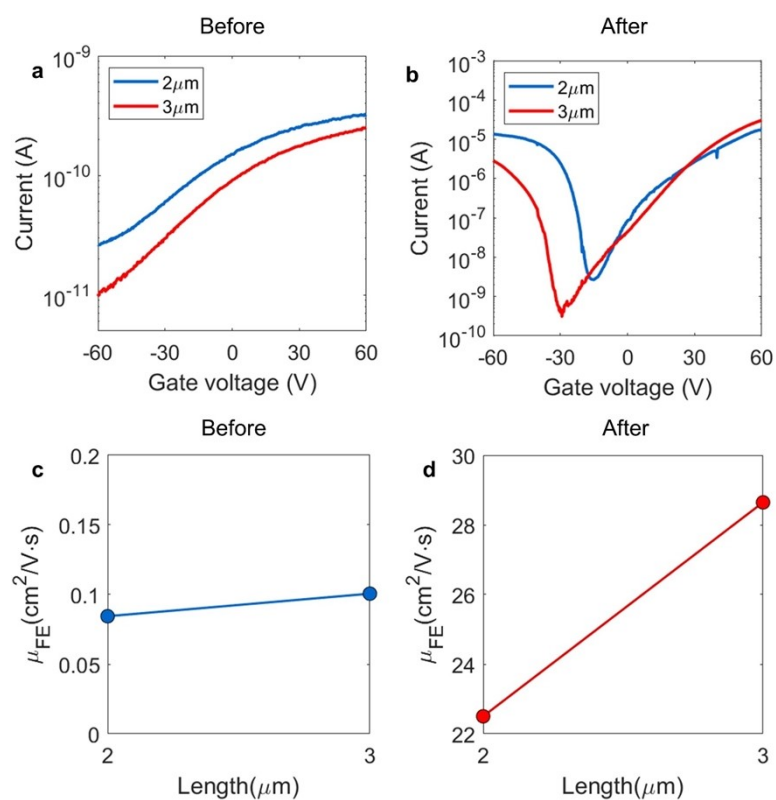
Figure S3 | The field effect mobility calculation with thinner WSe₂ devices. (a-b) Transfer characteristics of before and after self-propagation for the 40 nm thickness sample. **(c-d)** Calculated field effect mobility before and after the process.
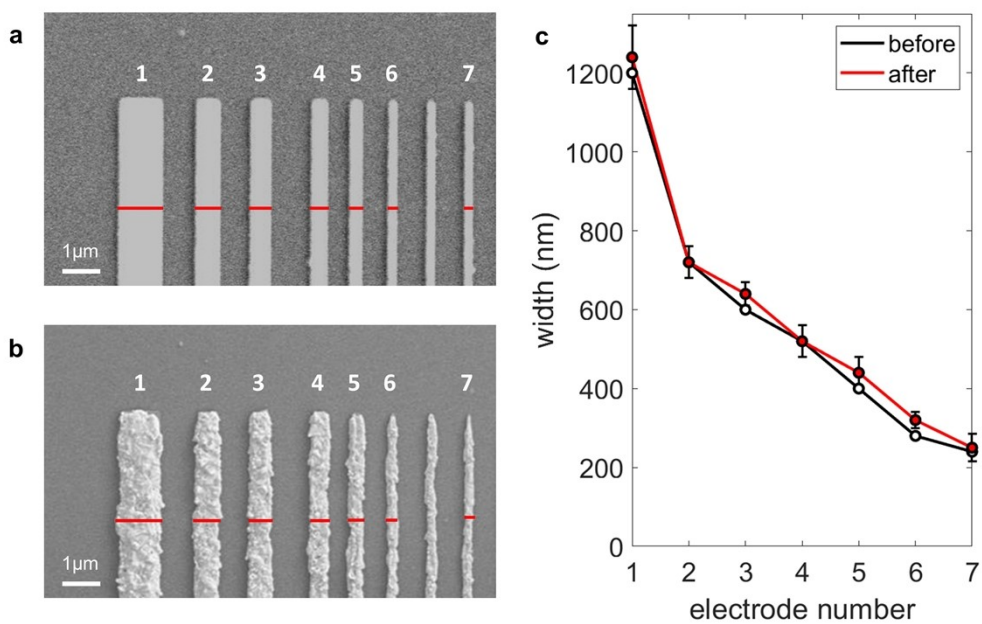
Figure S4 | SEM images of Field's metal electrodes and lateral propagation test. a-b, SEM images of electrodes before and after the self-propagation. **(c)** Width comparison after making Field's metal electrodes.
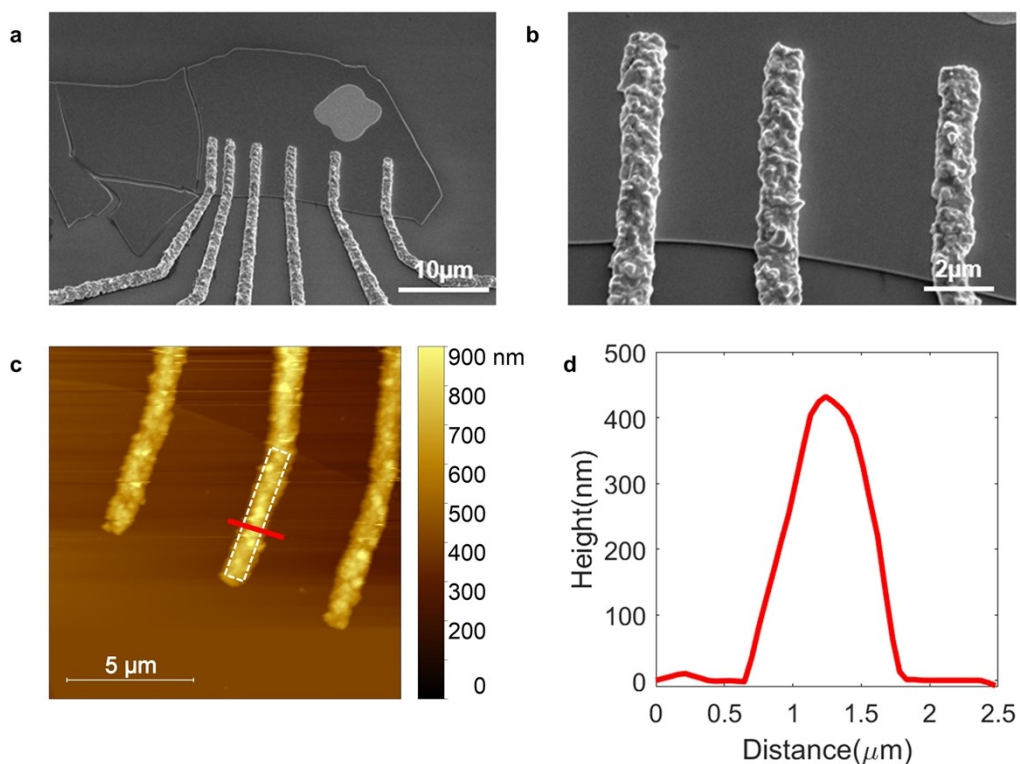
Figure S5 | Thickness distribution and surface roughness of Field's metal electrodes. a-b, Close SEM images after self-propagation. **(c)** AFM data of WSe_2 sample with Field's metal electrodes. **(d)** Line profile of the AFM result.
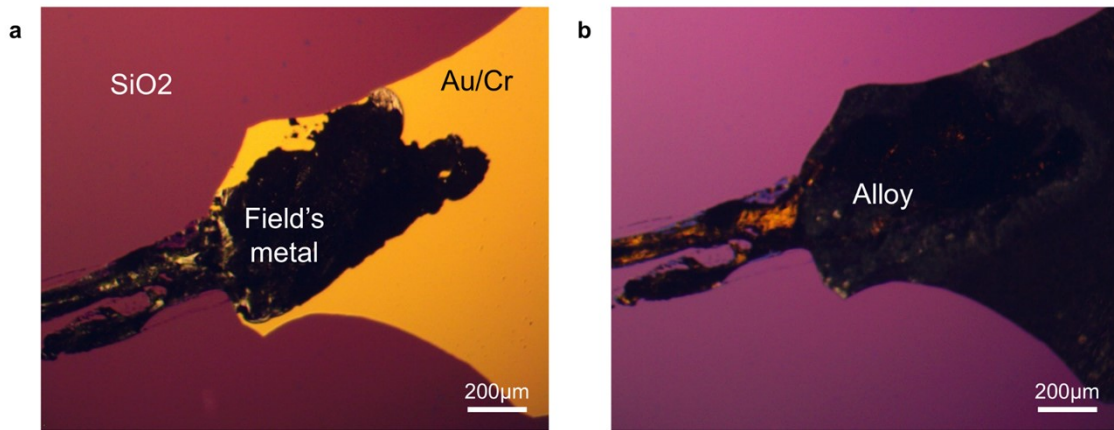
Figure S6 | Self-propagation in ambient pressure. (a) The optical image before annealing **(b)** after annealing at $300℃$, ambient pressure for 2 hours.
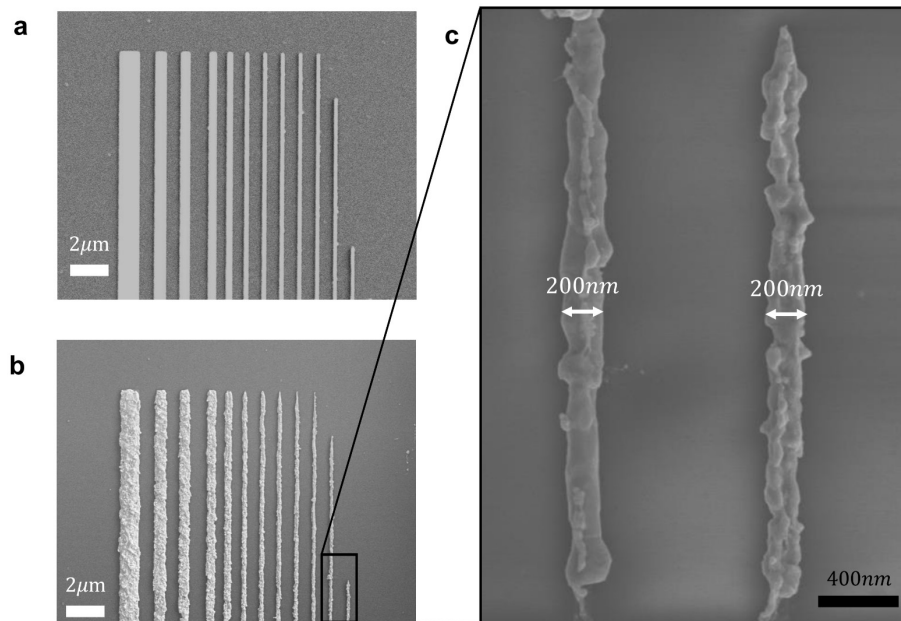
Figure S7 | Resolution test for Field's metal electrodes. a-b, SEM images of the test device. (**c**) Zoomed-in SEM image.
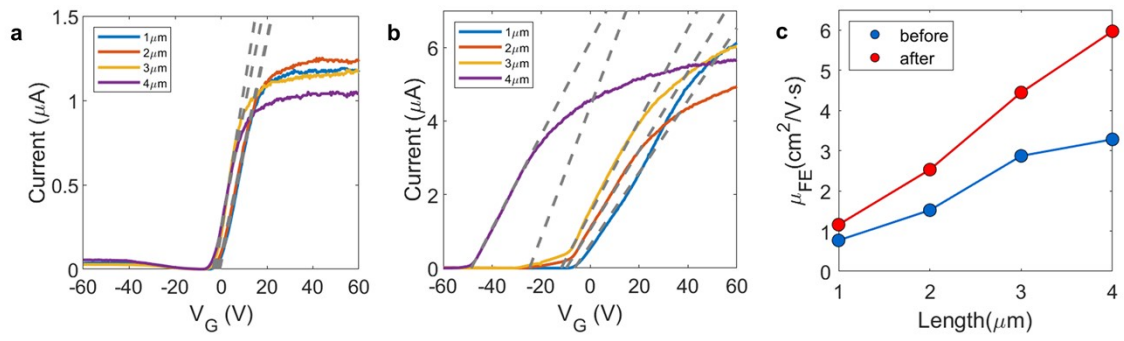
Figure S8 | Electrical characteristics and the field effect mobility calculation. a-b, Transfer characteristics ($I_{DS} - V_G$) of before and after self-propagation. **(c)** Calculated field effect mobility of the device.

Supporting Information Reference

1.	Das, S., Chen, H.-Y., Penumatcha, A. V. & Appenzeller, J. High Performance Multilayer MoS2 Transistors with Scandium Contacts. *Nano Lett.* **13**, 100–105 (2013).
2.	Li, S.-L. *et al.* Thickness-Dependent Interfacial Coulomb Scattering in Atomically Thin Field-Effect Transistors. *Nano Lett.* **13**, 3546–3552 (2013).
3.	Liu, B. *et al.* High-Performance Contact-Doped WSe2 Transistors Using TaSe2 Electrodes. *ACS Appl. Mater. Interfaces* **16**, 19247–19253 (2024).
4.	Tang, S.-Y., Lin, Y., Joshipura, I. D., Khoshmanesh, K. & Dickey, M. D. Steering liquid metal flow in microchannels using low voltages. *Lab Chip* **15**, 3905–3911 (2015).
5.	Wissman, J., Dickey, M. D. & Majidi, C. Field-Controlled Electrical Switch with Liquid Metal. *Advanced Science* **4**, 1700169 (2017).
6.	Joshipura, I. D., Ayers, H. R., Majidi, C. & Dickey, M. D. Methods to pattern liquid metals. *J. Mater. Chem. C* **3**, 3834–3841 (2015).
7.	Gozen, B. A., Tabatabai, A., Ozdoganlar, O. B. & Majidi, C. High-Density Soft-Matter Electronics with Micron-Scale Line Width. *Advanced Materials* **26**, 5211–5216 (2014).
8.	Boley, J. W., White, E. L., Chiu, G. T.-C. & Kramer, R. K. Direct Writing of Gallium-Indium Alloy for Stretchable Electronics. *Advanced Functional Materials* **24**, 3501–3507 (2014).
9.	Ladd, C., So, J.-H., Muth, J. & Dickey, M. D. 3D Printing of Free Standing Liquid Metal Microstructures. *Advanced Materials* **25**, 5081–5085 (2013).